DOI 10.1007/s10692-018-9954-7
Fibre Chemistry, Vol. 50, No. 3, September, 2018 (Russian Original No. 3, May-June, 2018)

X-RAY DIFFRACTION STUDY OF CELLULOSE POWDERS AND THEIR HYDROGELS. COMPUTER MODELING OF THE ATOMIC STRUCTURE

L. A. Aleshina,* A. I. Prusskii,*
A. M. Mikhailidi, and N. E. Kotel'nikova*****

UDC 661.728+542.8:004.94

Cellulose powders from flax fiber and deciduous wood and hydrogels regenerated from DMA/LiCl solutions of them were studied using x-ray diffraction. Structural characteristics were calculated. Three-dimensional models of atomic positions in the short-range order of amorphous hydrogels were constructed. It was found that flax cellulose was characterized by a higher degree of crystallinity and larger transverse cross section and monofilament length than deciduous cellulose. Super-swelled and lyophilized hydrogels from the cellulose solutions gave diffuse diffraction patterns characteristic of amorphous materials. The calculated coordination-sphere radii for lyophilized hydrogels corresponded to analogous data for cellulose II. Differences in the coordination numbers were due to structural differences in the short-range order. The distribution of atoms in the short-range ordered region was modeled using molecular dynamics and corresponded to a disordered cellulose II cluster with dimensions along the crystallographic axes of 2a, 2b, and 5c (15, 16, and 52 Å). A cluster consisted of 16 cellulose chains ~52 Å in length.

Hydrogels based on cellulose and its derivatives possess promising functional qualities. Hydrogels are three-dimensional (3D) materials that can absorb a large amount of H_2O. The 3D structure of swelled hydrogels is supported by a system of physical (physical gelation) or chemical (chemical gelation) cross links.

Structural studies of cellulosic materials have a long history starting with the emergence of polymer science. All four cellulose allomorphs (polymorphic modifications I-IV) have systems of H-bonds formed by cellulose hydroxyls. Natural cellulose exists in two different crystalline phases, Iα and Iβ. Both belong to the cellulose I polymorph. The crystalline phase Iα is found primarily in cell walls of certain algae and in bacterial cellulose. Phase Iβ is found mainly in higher plants and is more stable than Iα. Layers of parallel H-bonded cellulose chains are common to both crystalline phases and represent a key parameter of the cellulose structure. The main difference between phases Iα and Iβ is the variation of these layers relative to each other along the chain direction [1].

Cellulose II (CII) is yet another very important crystalline phase of cellulose. It is synthesized from cellulose I by mercerization and regeneration from solutions.

The degree of crystallization (DC) is used to characterize the structural ordering of cellulose, is known to reflect the ratio of amorphous and crystalline sections in its structure, and is determined using x-ray diffraction. The DC is a relative quantity because the obtained values depend on the calculation method.

X-ray diffraction studies of amorphous polymers can provide structural information about molecular fragments and the nature of their mutual positioning in the short-range ordered region. Computer modeling can solve the problem of establishing the nature of the mutual positioning of the molecular fragments. Herein, two types of celluloses were used, i.e., cellulose powders (CPs) isolated from flax fiber and deciduous wood and hydrogels regenerated from solutions of these celluloses in DMA/LiCl.

Until now, x-ray studies of super-swollen and dried cellulose hydrogels were limited to qualitative discussions of the changes in the diffraction patterns. Thus, swelling of softwood cellulose dissolved in DMA/LiCl and regenerated

*Petrozavodsk State University; **St. Petersburg State University of Industrial Technologies and Design; ***Institute of Macromolecular Compounds, Russian Academy of Sciences, St. Petersburg. E-mail: amikhailidi@yahoo.com. Translated from *Khimicheskie Volokna*, No. 3, pp. 28-36, May—June, 2018.

 0015-0541/18/5003-0166© 2018 Springer Science+Business Media LLC

using two different anti-solvents was studied [2]. The results showed that the crystalline structure of softwood cellulose was lost after swelling, dissolution, and subsequent isolation of the solid. The transformation of microcrystalline cellulose during its partial dissolution in DMA/LiCl was studied and allowed the disappearance of diffraction from crystals in samples that were dried after being saturated with H_2O to be explained by formation of very small or defective crystals during slow isolation of the solid [3]. It is noteworthy that samples regenerated from solutions were lyophilized or thermally dried after isolation in both above examples. This led to partial or complete loss of H_2O and formation in the isolated phase of a new structure that was usually different from cellulose I of the dissolved samples. Modern methods for analyzing x-ray diffraction results allowed the secondary structures formed during drying to be characterized.

The goals of the present work were an x-ray study of cellulose powders and hydrogels, calculation of the structural characteristics, and computer modeling of the atomic structure of the lyophilized hydrogels.

Experimental

CP samples were obtained from wastes of flax fiber (FC) and bleached softwood cellulose (WC) using acid hydrolysis. CPs were dissolved in DMA/LiCl. Their solubility was up to 99.8 mass%. Hydrogels were prepared from the solutions by self-assembly of cellulose chains during spontaneous gelation. Details of the methods for preparing the samples and their physicochemical properties were published [4, 5].

X-ray studies used three types of samples, i.e., CP, super-swollen CP hydrogels, and lyophilized hydrogels.

X-ray patterns were recorded on a DRON diffractometer using Fe and Mo Kα-radiation in reflection and transmission geometries. CP samples were pressed tablets, the thickness of which (~0.08 cm) allowed x-ray patterns to be obtained in transmission geometry. Super-swollen hydrogels were handled constantly in a moist medium so that they did not dry out during recording of the x-ray patterns. Scattering angles from 12.2 to 34° were used for the measurements.

The supramolecular characteristics of the cellulosic materials that were calculated from the x-ray patterns were the degree of crystallinity (DC) and sizes of coherent scattering regions (CSRs) (regions of crystallinity or crystallites). The DC of samples was calculated using the Ruland method [6]. The sizes of the CSRs were also estimated.

Calculation of cellulose supramolecular characteristics

The DC is traditionally viewed as the ratio of the integrated scattering intensity of crystalline cellulose to the total integrated scattering intensity of the studied sample [7]. The method for calculating the DC of cellulose and its derivatives from the diffraction patterns was based on a geometric order model of the molecular positions, i.e., long-range order in the coherent scattering regions (CRSs) and short-range order in the amorphous component, and has been used in many publications [7-12]. The Ruland [6] or Segal method [8] was used in most of them. The method for calculating the DC that was used in the present work was similar to the Ruland method and was described and justified in detail [11, 12].

Sizes of crystalline regions were calculated using the Scherrer formula [8, 9, 11]

$$\beta_{hkl} = \frac{0{,}9\lambda}{D_{hkl}\cos\theta}, \tag{1}$$

where β_{hkl} is the integrated width of the reflection with indices *hkl* (deg); λ, wavelength of incident light; D_{hkl}, effective size of the CSR in the direction normal to the reflecting planes.

The envelopes of x-ray reflections must be approximated using any approximating function in order to calculate the sizes of the CSRs from their widths. The actual D_{hkl} values are known to lie within a range calculated by Gaussian and Cauchy approximation. Both approximations were used in the work. The resulting D_{hkl} values were calculated as averages. The contributions to the reflection widths due to the exposure geometry were taken into account using the Jones method (standard) [12].

Figure 1 shows directions [*hkl*] along which the sizes of crystallinity regions D_{hkl} were calculated from the widths of reflections with indices *hkl*. It can be seen that the shape of the transverse cross section of monofilaments was determined from the CSR sizes in the directions $[1\bar{1}0]$, [110], and [100], which lay in the basal plane of the unit cell. The length of the CSR in the fibril axial direction was the CSR size in the [001] direction.

Calculation of short-range order characteristics

Structural characteristics of the amorphous material such as the radial distribution functions of atoms or electrons were determined from the diffraction data. The coordination sphere radii r_{ij} and coordination numbers N_{ij} could be calculated if these functions were known. The pairing functions method was developed by the Norwegian school of Finbak [13] and applied by Warren to the interpretation of results for simple oxides [14-16]. The specifics of applying this method to cellulosic items was discussed before [17].

Normalized experimental scattering intensities $I_{\exp}(s)$ ($s = 4\pi\sin\theta/\lambda$ is the length of the diffraction vector) were used to calculate s, weighted interference function $H(s)$:

$$H(s) = s\left[I_0(s) - \sum_{l=1}^{M} f_f^2(s)\right]\exp(-\alpha^2 s^2)\, g^{-2}(s), \tag{2}$$

where $f_j(s)$ is the atomic scattering function of the atom with number j; $g^2(s)$, a sharpening factor; α, coefficient in the decay factor that decreases the influence of experimental error at large s values; and r_{ij}, coordination sphere radii.

The Finbak—Warren method allows $D(r)$ calculated from the electron radial distribution function $H(s)$ to be written as the sum of effective pairing functions $P_{ij}2(r)$:

$$D(r) = 2\pi^2 r\rho_{\text{el.}}(r) = \sum_i \sum_j \frac{N_{ij}}{r_{ij}} P'_{ij}(r) = \int_0^{s_{\max}} H_s\, ds. \tag{3}$$

Pairing function $P_{ij}2(r)$ characterizes the electron-density distribution of a single separately chosen pair of atoms considering the variability of each coordination sphere $\sigma_{ij}(s)$ in the amorphous system. This enables the coordination numbers N_{ij} to be calculated by least-squares (LS) methods, refining in parallel by trial and error the radii r_{ij} and variabilities σ_{ij} of the coordination spheres [17].

Computer model build

Computer modeling was used to determine the mutual positioning of the molecular fragments from the x-ray diffraction data. Previous results [18, 19] and a comparison of diffraction patterns of xerogels with those calculated for cellulose Iβ and II found that the structure of cellulose hydrogels regenerated from CP solutions in DMA/LiCl was based on the positioning motif of cellulose II chains. Therefore, the starting model was built by translating the cellulose II unit cell in the directions of crystallographic axes x, y, and z. Cellulose II has a monoclinic unit cell with constants $a = 8.01$, $b = 9.04$, and $c = 10.36$ Å and angle $\gamma = 117.1°$ [20]. Then, the starting model was optimized according to Polak—Ribiere and relaxed using molecular dynamics in the HyperChem 8 program, which can model the electronic and atomic structure of complicated molecular systems.

The MM+ force field that is basic to the HyperChem 8 program [21-23] and is an improved version of the MM2 method developed for organic molecules was chosen to minimize the cluster energy.

Force fields of the MM type were demonstrated to be adequate for building cellobiose computer models [24]. MM+ is used comparatively rarely for conformational analysis of carbohydrates. Nevertheless, several encouraging results were obtained using it [25]. Thus, this method was used successfully to build an atomic model of amorphous softwood cellulose sulfate obtained via regeneration from DMA/LiCl solutions [19].

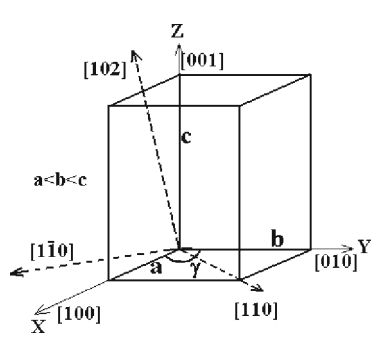

Fig. 1. Orientation of unit-cell axes and several crystallographic directions in the cellulose 1β lattice [12].

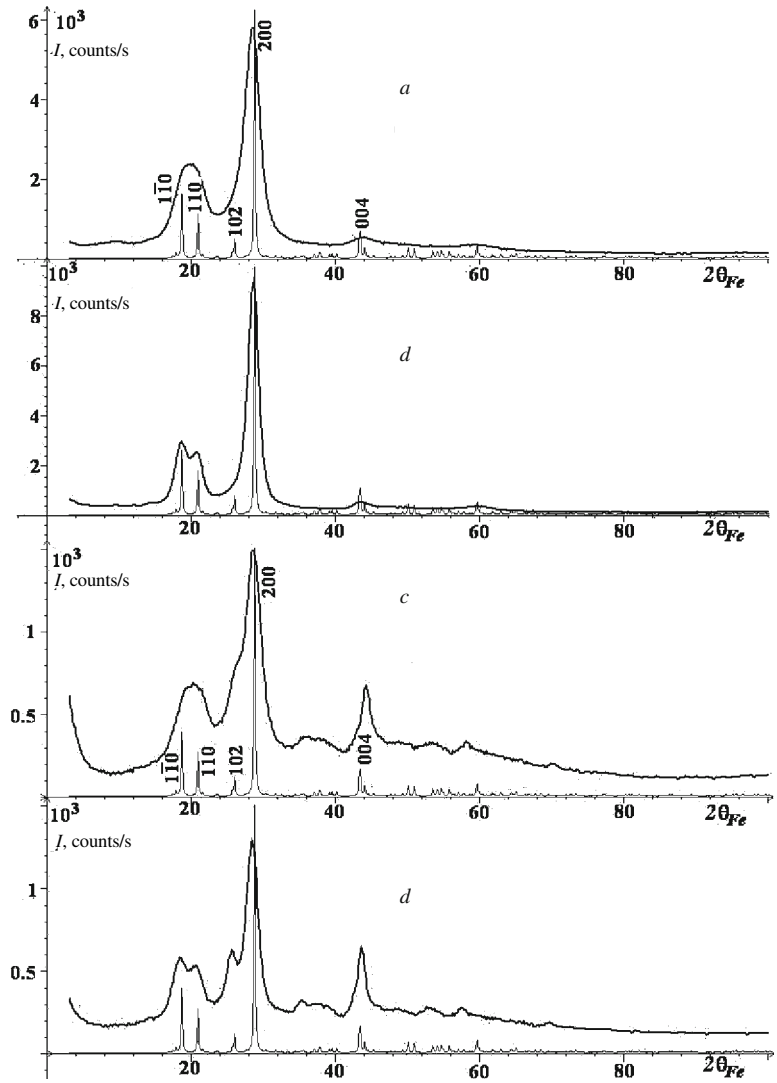

Fig. 2. X-ray diffraction patterns of wood (a, c) and flax CP (b, d) recorded in reflection (a, b) and transmission geometry (c, d) compared with the published x-ray pattern calculated theoretically from atomic coordinates of cellulose Iβ [26].

The agreement of the resulting model and the experiment was monitored by comparing the experimental intensity distribution $I(s)$, s-weighted interference function $H(s)$, radial atomic distribution function $W(r)$, and coordination sphere radii and numbers with those calculated from the atomic coordinates of the built model.

The scattering intensity distributions obtained for the model atomic configuration $I(s)_{\text{mod}}$ were calculated using the Debye formula for each configuration of the molecular system in the HyperChem 8 program [12, 17]. The agreement level of intensity scattering curves calculated for the model $I(s)_{\text{mod}}$ and the experimental $I(s)_{\text{exp}}$ was estimated as before [19] by calculating the profile uncertainty factors:

$$R_p = \frac{\sum \left| I(s)s_{\text{exp}} - I(s)_{\text{mod}} \right|}{\sum I(s)_{\text{mod}}}. \tag{4}$$

Distribution curves of pairing functions $D(r)_{\text{mod}}$ and s-weighted interference functions $H(s)_{\text{mod}}$ were calculated from the $I(s)_{\text{mod}}$ curves using Eqs. (2) and (3).

The function $W(r)$ was used instead of $D(r)$ to compare the experimental results with those calculated for clusters and was written

Table 1. DC and CSR Sizes of FC and WC from X-ray Patterns Recorded in Reflection (1) and Transmission Geometry (2). Average D_{hkl} Values Calculated by the Gaussian and Cauchy Methods Are Given

Sample		Deciduous CP		Flax CP	
		1	2	1	2
DC, ±5%		74	79	86	87
[*hkl*]	(*hkl*)	D_{hkl}, Å; $\Delta D_{hkl} = \pm 5$ Å			
$1\bar{1}0$	$1\bar{1}0$	32	32	60	47
110	110	61	61	60	60
100	200	48	48	86	62
001	004	35	90	90	155

$$W(r) = \frac{D(r)}{2\pi^2 r \rho_e \sum_j x_j}. \tag{5}$$

According to Eq. (3), the experimental function $D(r)$ oscillated near the straight line $D_0(r) = 2\pi^2\rho_e\Sigma_j z_j$, the slope of which was determined by the average electron density ρ_e. The $D(r)_{mod}$ curve calculated for the model oscillated near the parabola $D_0(r)_{mod}$ because of the small size of the model. Function $D(r)_{mod}$ was calculated from intensity distribution curve $I(s)_{mod}$ at the upper limit of s values, equal to 1 Å^{-1}. As a result,

$$W(r)_{mod} = \frac{D(r)_{mod}}{D_0(r)_{mod}}. \tag{6}$$

and the shape of the $W(r)$ curve calculated using Eqs. (5) and (6) was independent of the nature of the average electron-density distribution.

Analysis of x-ray patterns of starting cellulose powders

Figure 2 shows x-ray patterns of softwood and flax CPs that were taken using Fe Kα-radiation. The theoretically calculated x-ray pattern of cellulose Iβ is given for comparison. The indices of the main reflections are shown for the model structure of cellulose Iβ with cell constant $a < b$, the c axis directed along the fibril axis, and monoclinic angle γ.

Figure 2 shows that the positions of reflection maxima $(\bar{1}10)$, (110) and (102), (200) were separated in the x-ray pattern of flax cellulose and that the (004) reflection was narrow and strong. The cellulose samples scattered because the fibrils were oriented primarily anisotropically. This was indicated by differences in diffraction patterns recorded in reflection and transmission geometry. The DC calculated for FC was 10% greater than that for WC (Table 1).

The sizes of the CSRs (crystalline regions) were calculated for four crystallographic directions [*hkl*] in the cellulose Iβ lattice, $[1\bar{1}0]$ and [110] (along the unit-cell basal-plane diagonal), [100] (along the a axis), and [001] (along the c axis and the fibril axis), from the reflection widths with indices (*hkl*) $[1\bar{1}0]$, (110), (200), and (004), respectively. The crystallite fibril CSR along an axis perpendicular to the sample surface (reflection geometry) was almost three times greater for FC than for WC. The size of the CSR in the direction of the fibril axis for crystallites with axes parallel to the sample surface (transmission geometry) was 1.7 times greater for FC than WC.

Figure 3 shows the shapes of the transverse cross sections of monofilaments (cross section of unit-cell plane *ab* perpendicular to the fibril axis) that were built using the D_{hkl} values. The cross-sectional dimensions of elemental fibrils obtained from the x-ray data were characteristically close to hexagonal. This agreed with previously proposed models [27, 28] and atomic-force spectroscopic data [29]. Figure 3 shows that the cross-sectional area (CSA) of monofilaments of both types of cellulose were independent of the sample orientation relative to the incident rays. The CSA of WC elemental fibrils was less than that of FC. However, the linear sizes in the [110] direction, which coincided with the shorter diagonal of the basal plane of the monoclinic unit cell of cellulose 1β, were similar.

Thus, the sizes of the ordered regions along the elemental fibrils were 1.7 times greater for FC than for WC. The CSA of elemental fibrils and the DC of FC were greater than those for WC.

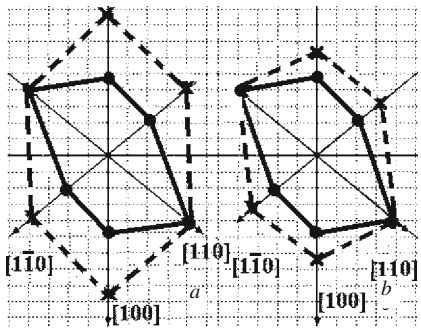

Fig. 3.

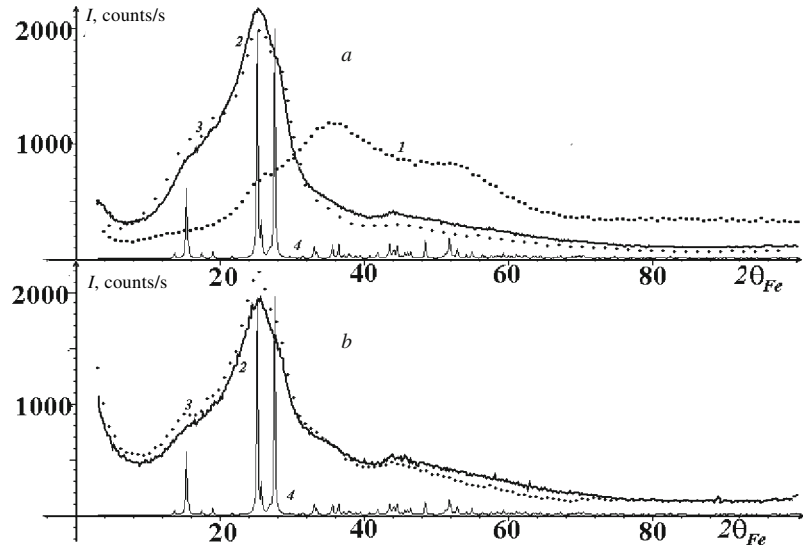

Fig. 4.

Fig. 3. Diagrams of cross sections of monofilaments of wood (%) and flax cellulose (×) in the plane perpendicular (reflection geometry) (a) and parallel (transmission geometry) to the sample surface (b).

Fig. 4. Diffraction patterns of super-swelled WC (1) and lyophilized WC (2) and FC hydrogels (3) recorded in reflection (a) and transmission geometry (b) and x-ray pattern of cellulose II (4).

Analysis of x-ray patterns of super-swollen and lyophilized hydrogels of wood and flax CPs

Figure 4 shows x-ray patterns of super-swollen and lyophilized WC hydrogels and lyophilized FC hydrogel as compared with that calculated for CII in previous work [26, 30].

X-ray patterns of super-swollen and lyophilized hydrogels were diffuse, indicating that they were amorphous. Swollen hydrogels gave maxima in the x-ray patterns that were shifted and broadened as compared with those of lyophilized samples because of the large amount of water in them [31].

The intensity in the small-angle region of transmission x-ray patterns was greater than that recorded in reflection geometry. Apparently, this was explained by the existence of electron-density irregularities in the direction parallel to the sample surface.

Calculation of short-range order characteristics of lyophilized hydrogels of WC and FC

X-ray patterns of lyophilized gels were taken using Mo Kα-radiation in order to calculate the coordination sphere radii and coordination numbers because this increased the region of inverse space in which the scattering curve was recorded and improved the resolution of the electron-density scattering curve. Figure 5 shows the corresponding normalized scattering intensity distribution curves $I(s)$ and the s-weighted interference function $H(s)$ and pairing functions $D(r)$ calculated from them.

Table 2 presents the calculated short-range order characteristics, i.e., radii r_{ij}, broadening σ_{ij} of coordination spheres, and coordination numbers N_{ij} for lyophilized WC and FC hydrogels as compared with the theoretically calculated values for CII. Factor q characterized the agreement level of the experimental distribution curves of pairing functions $D(r)$ and curves $D_{mic}(r)$ that were calculated from the radii r_{ij}, broadenings σ_{ij} of coordination spheres, and coordination numbers N_{ij} found by least-squares methods.

Here q is the discrepancy level of the $D(r)$ and $D(r)_{mic}$ curves shown in Fig. 6. The last was calculated from the r_{ij}, N_{ij}, and σ_{ij} values given in Table 2. Table 2 and the $D(r)$ curves show that although the coordination-sphere radii coincided practically identically with the data for CII, the coordination number and $D(r)$ curves calculated for FC and WC differed both among themselves and from the corresponding data for CII. The discrepancies in the coordination

Table 2. Short-range Order Characteristics of WC and FC Compared with Analogous Data for Cellulose II (CII)

	r_{ij}, Å			N_{ij}, at.			σ_{ij}, Å	
	WC	FC	CII	WC	FC	CII	WC	FC
CO_1	1.45	1.41	1.42	1.1	0.4	1.2	0.10	0.08
CC_1	1.51	1.50	1.51	1.1	2.2	1.7	0.08	0.00
OH	–	1.90	–	–	8.0	–	–	0.00
CO_2	2.37	2.37	2.37	2.2	1.1	2.3	0.30	0.00
CC_2	2.49	2.43	2.47	3.9	2.4	2.0	0.10	0.20
OO_1	2.86	2.82	2.86	2.6	4.9	3.2	0.12	0.30
CO_3	3.08	3.20	3.02	1.2	0.9	2.5	0.01	0.20
CC_3	3.62	3.62	3.61	13.3	12.6	2.4	0.30	0.30
OO_2	3.65	3.80	3.72	1.3	1.9	3.5	0.10	0.10
CO_4	4.10	4.10	4.02	4.9	3.4	3.3	0.20	0.20

$\Delta r_{ij} = \pm 0.01$ Å, $\Delta N_{ij} = \pm 0.1$ at.; $q = 5\%$.

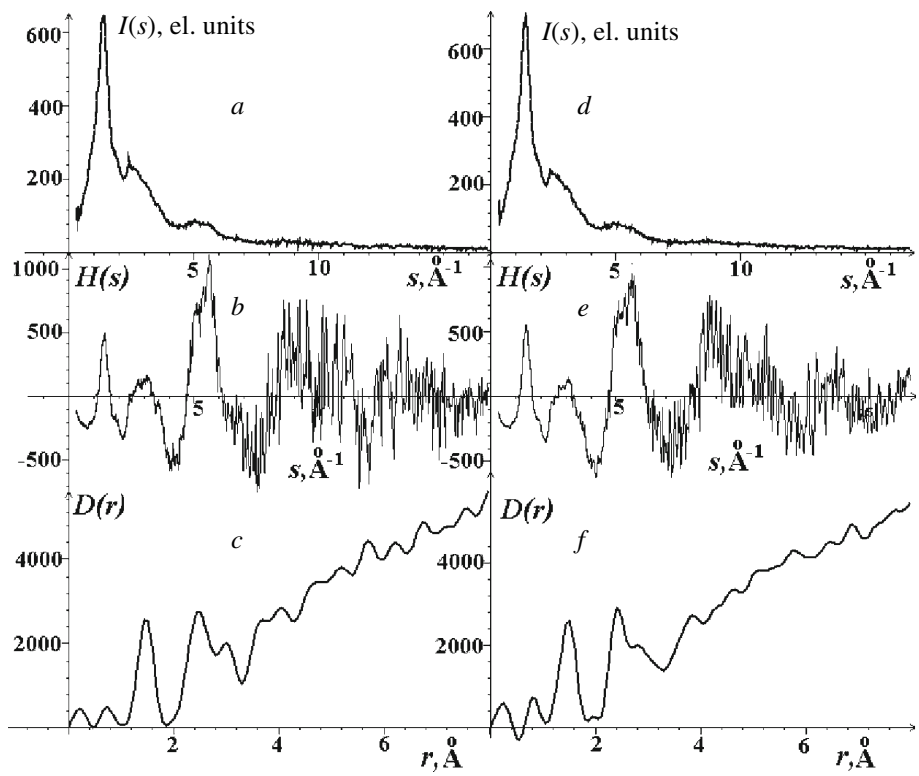

Fig. 5. Scattered-intensity distribution curves $I(s)$, s-weighted interference function $H(s)$, and pairing functions $D(r)$ of lyophilized hydrogels: WC (a, b, c) and FC (d, e, f).

number were due to destruction of long-range order and the presence of residual water in the lyophilized hydrogels.

Computer modeling of the atomic structure of lyophilized WC hydrogel

Further discussion of the experimental results requires building three-dimensional models of atomic positions within the short-range ordering. Starting models were built by translating the CII unit cell in the directions of the x, y, and z crystallographic axes.

Table 3. Short-range Order Characteristics of Final Cluster Model Compared with Corresponding Data for Cellulose II

Sphere type	$r_{ij\,\mathrm{exp.}}$	$r_{ij\,\mathrm{mod.}}$	r_{ij} (CII)	$N_{ij\,\mathrm{exp.}}$	$N_{ij\,\mathrm{mod.}}$	N_{ij} (CII)	σ_{ij}
C-O1	1.45	1.44	1.41	1.05	1.15	1.1	0.1
C-C1	1.51	1.55	1.54	1.06	1.67	1.6	0.08
C-O2	2.37	2.47	2.41	2.18	1.77	3.9	0.3
C-C2	2.49	2.52	3.85	3.96	1.97	1	0.1
O-O1	2.86	2.82	2.86	2.61	2.6	2.86	0.12

$\Delta r_{ij} = \pm 0.01$ Å; $\Delta N_{ij} = \pm 0.1$ at.

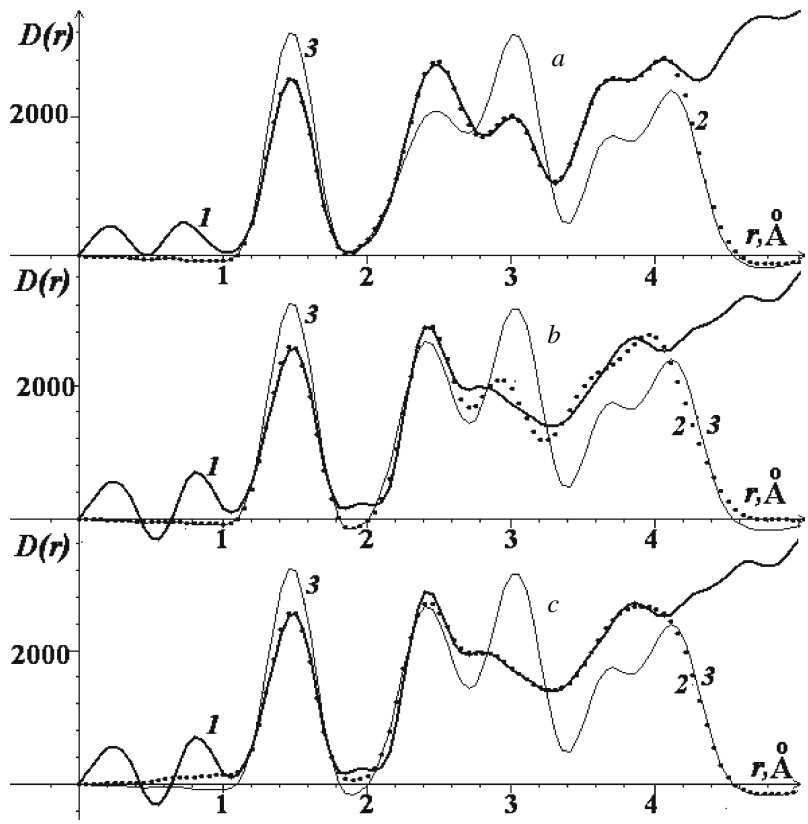

Fig. 6. Experimental curves for $D(r)$ (1), $D(r)_{\mathrm{mic}}$ (····) (2), and $D(r)_{\mathrm{theor}}$ (3) for cellulose II: WC hydrogel (a); FC hydrogel (b, c); calculation without (b) and with (c) considering the appearance of a sphere with $r = 1.9$ Å. $D(r)_{\mathrm{theor}}$ was calculated from the r_{ij}, σ_{ij}, and N_{ij} values for cellulose II.

The number of translations varied widely. In each instance, the models were geometrically optimized by the Polak—Ribiere method, relaxed using molecular dynamics, and again geometrically optimized. The final model corresponded to 2, 2, and 5 translations. The uncertainty factor calculated using Eq. (4) was 0.07, the lowest value of all built models.

The $H(s)$ and $W(r)$ curves calculated from the experiment with the studied sample and the cluster model with 2, 2, and 5 translations agreed well after molecular dynamics and geometric optimization (Figs. 7 and 8).

Short-range order characteristics of the model built for lyophilized WC hydrogel, i.e., radii r_{ij}, broadening σ_{ij} of the coordination spheres, and coordination numbers N_{ij}, were calculated for the final cluster. Table 3 presents the results of the calculations.

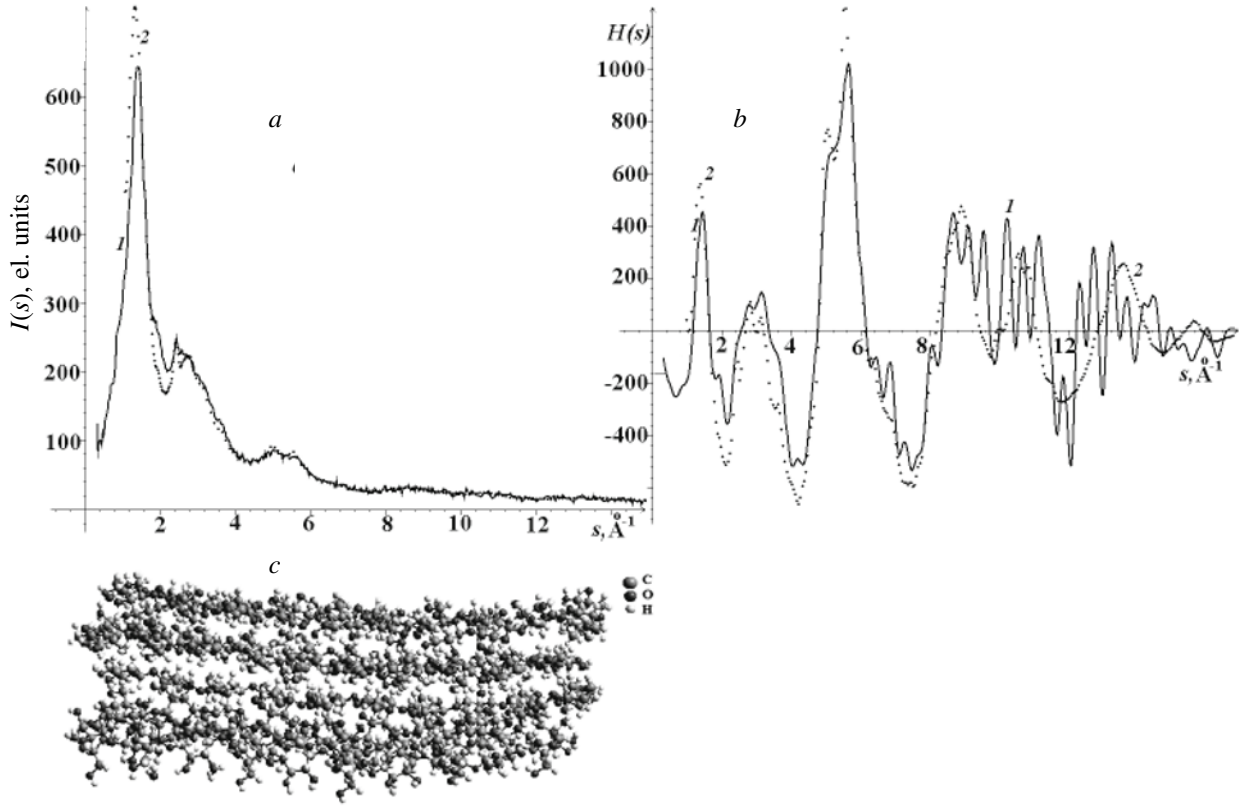

Fig. 7. Scattering intensity (a) and *s*-weighted interference functions (b) of FC hydrogel (1) and the calculated final structure model shown in the figure (2) (c).

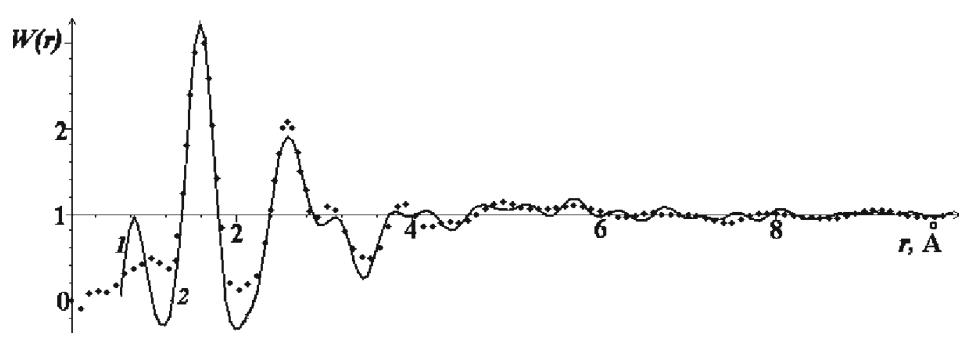

Fig. 8. Atomic radial distribution functions $W(r)$ calculated for the experiment (1) and model (2).

Table 3 shows that the coordination-sphere radii of the model and experiment agreed. The coordination numbers for the model were close to those for CII. Apparently, the slight discrepancies were related to the fact that the presence of a small amount of water in the lyophilized hydrogels was not considered at this stage of model building.

Thus, the cellulose cluster with 2, 2, and 5 translations gave the lowest uncertainty factor and best agreement of the experimental and model scattering intensity distribution curves, *s*-weighted interference function, atomic radial distribution function, and coordination-sphere radii and coordination numbers. The coordination-sphere radii for lyophilized hydrogels agreed in general with the analogous values for CII. The model of the atomic distribution in the short-range ordering region that was calculated by molecular dynamics corresponded to a disordered cluster of CII with dimensions along the crystallographic axes of 2*a*, 2*b*, and 5*c* (15, ~16, and 52 Å). A cluster consisted of 16 cellulose chains ~52 Å in length.

REFERENCES

1. M. Wada, Y. Nishiyama, et al., *Adv. X-ray Anal.*, 51, 138-144 (2008).
2. J. Obradovic, H. Wondraczek, et al., *Cellulose*, 21, No. 6, 4029 (2014).
3. B. J. C. Duchemin, R. H. Newman, and V. P. Steiger, *Cellulose*, 14, 311-320 (2007).
4. N. E. Kotelnikova, Yu. V. Bikhovtsova, et al., *Cellul. Chem. Technol.*, 48, 643-651 (2014).
5. N. Kotelnikova, A. Mikhailidi, et al., *Cellul. Chem. Technol.*, 50, No. 5-6, 545-555 (2016).
6. W. Ruland, *Acta Crystallogr.*, 14, 1180-1185 (1961).
7. A. Thygesen, J. Oddershede, et al., *Cellulose*, 12, 563-576 (2005).
8. X. Ju, M. Bowden, et al., *Carbohydr. Polym.*, 123, 476-481 (2015).
9. P. Ahvenainen, I. Kontro, and K. Svedstrom, *Cellulose*, 23, 1073-1086 (2016).
10. N. Terinte, R. Ibbett, and K. C. Schuster, *Lenzinger Ber.*, 89, 118-131 (2011).
11. M. F. Torlopov, V. I. Mikhaylov, et al., *Cellulose*, 25, 1031-1046 (2018).
12. N. V. Melekh, "X-ray Structural Studies of Celluloses and Lignins of Various Origins," Candidate Dissertation, PetrGU, Petrozavodsk, 2008, 166 pp.
13. B. E. Warren, *X-ray Diffraction*, Addison-Wesley Publ. Co., Reading, Mass., 1969, 381 pp.
14. B. E. Warren, *Kristallografiya*, 16, No. 7, 1264-1270 (1971).
15. R. L. Mozzi and B. E. Warren, *J. Appl. Crystallogr.*, 2, No. 1, 164-170 (1969).
16. R. L. Mozzi and B. E. Warren, *J. Appl. Crystallogr.*, 3, No. 2, 251-358 (1970).
17. N. V. Melekh, *Natural and Technical Cellulose. Structure Analysis* [in Russian], Izd. LAP, Moscow, 2013, 104 pp.
18. C. Yamane, T. Aoyagi, et al., *Polym. J.*, 38, No. 8, 819-826 (2006).
19. A. I. Prusskii and L. A. Aleshina, *Vysokomol. Soedin., Ser. A*, 57, No. 3, 268-281 (2016).
20. P. Langan, Y. Nishiyama, and H. Chanzy, *Biomacromolecules*, 2, 410-416 (2001).
21. G. I. Kobzev, *Application of Non-empirical and Semi-empirical Methods in Quantum-Chemical Calculations: Student Aide* [in Russian], Gos. Orenburgskii Univ., Orenburg, 2004, 150 pp.
22. C. Stan Tsai, *An Introduction to Computational Biochemistry*, Wiley-Liss, New York, 2002, 368 pp.
23. M. E. Solov'ev and M. M. Solov'mev, *Computational Chemistry* [in Russian], SOLON-Press, Moscow, 2005, 536 pp.
24. C. A. Stortz, G. P. Johnson, et al., *Carbohydr. Res.*, 344, 2217 (2009).
25. A. G. Gerbst, A. A. Grachev, et al., *Bioorg. Khim.*, 33, No. 1, 28 (2007).
26. Y. Nishiyama, P. Langan, and H. Chanzy, *J. Am. Chem. Soc.*, 124, 9074-9082 (2002).
27. L. H. Thomas, V. T. Forsyth, et al., *Plant Physiol.*, 161, 465-476 (2013).
28. R. A. Festucci-Buselli, W. C. Otoni, and C. P. Joshi, *Braz. J. Plant Physiol.*, 19, No. 1, 1-13 (2007).
29. A. A. Baker, W. Helbert, et al., *Biophys. J.*, 79, 1139-1145 (2000).
30. N. V. Melekh and L. A. Aleshina, *Estestv. Tekh. Nauki*, No. 3, 37-43 (2011).
31. L. A. Aleshina and I. V. Lyukhanova, *Uch. Zap. Petrozavodsk. Gos. Univ., Ser. Estestv. Tekh. Nauki*, No. 6 (111), 55-60 (2010).